

# Quantum phase transitions in the dimerized extended Bose-Hubbard model

Koudai Sugimoto,<sup>1</sup> Satoshi Ejima,<sup>2</sup> Florian Lange,<sup>2</sup> and Holger Fehske<sup>2</sup>

<sup>1</sup>*Center for Frontier Science, Chiba University, Chiba 263-8522, Japan*

<sup>2</sup>*Institut für Physik, Universität Greifswald, D-17489 Greifswald, Germany*

(Dated: March 12, 2022)

We present an unbiased numerical density-matrix renormalization group study of the one-dimensional Bose-Hubbard model supplemented by nearest-neighbor Coulomb interaction and bond dimerization. It places the emphasis on the determination of the ground-state phase diagram and shows that, besides dimerized Mott and density-wave insulating phases, an intermediate symmetry-protected topological Haldane insulator emerges at weak Coulomb interactions for filling factor one, which disappears, however, when the dimerization becomes too large. Analyzing the critical behavior of the model, we prove that the phase boundaries of the Haldane phase to Mott insulator and density-wave states belong to the Gaussian and Ising universality classes with central charges  $c = 1$  and  $c = 1/2$ , respectively, and merge in a tricritical point. Interestingly we can demonstrate a direct Ising quantum phase transition between the dimerized Mott and density-wave phases above the tricritical point. The corresponding transition line terminates at a critical end point that belongs to the universality class of the dilute Ising model with  $c = 7/10$ . At even stronger Coulomb interactions the transition becomes first order.

## I. INTRODUCTION

Over the past years, ultracold atoms in optical lattices have become a fascinating tool to explore strongly correlated many-body systems and thereby provide also valuable insights into complex phenomena in solid-state systems [1–3]. Ultracold-atom-based quantum simulators have already been used, e.g., to observe the transition from a superfluid (SF) to a Mott insulator (MI) phase for bosons [4], to realize the crossover between Bose-Einstein condensation and Bardeen-Cooper-Schrieffer pairing [5], or to modulate the range of interactions in quantum systems [6, 7].

One of the targeted model systems for ultracold atoms is the Bose-Hubbard model (BHM), which has been intensively studied from a theoretical point of view. Quite recently, triggered by the observation of a symmetry-protected-topological (SPT) Haldane phase in the spin-1 Heisenberg chain [8–10], the related Haldane insulator (HI) phase in the extended BHM (EBHM) with longer-range repulsion [11] has attracted significant attention.

Including a bond dimerization, which can also be realized in optical lattices [12], the physical properties of the spin-1 chain change drastically, e.g., the Haldane phase shrinks rapidly when the dimerization increases and eventually even disappears [13, 14]. In this work, we explore the effect of the bond dimerization  $\delta$  in the EBHM using the density-matrix renormalization group (DMRG) technique [15, 16]. We especially demonstrate that a direct continuous transition takes place between the dimerized MI and density-wave (DW) phases, instead of the first-order transition observed in the pure EBHM ( $\delta = 0$ ).

The paper is structured as follows: Section II introduces the EBHM with bond dimerization, as well as the numerical techniques for its investigation. The physical quantities of interest will be defined in Sec. III. Section IV presents the ground-state phase diagram of the dimerized EBHM for  $\rho = 1$  and classifies the phase boundaries.

Some results for band filling factor  $\rho = 1/2$  can be found in Appendix A. Section V summarizes our results and gives a brief outlook.

## II. MODEL AND METHOD

As outlined above, we consider the EBHM with an additional explicit bond dimerization  $\delta$ ,

$$\hat{H} = \hat{H}_{\text{EBHM}} - t \sum_j \delta (-1)^j \left( \hat{b}_{j+1}^\dagger \hat{b}_j + \text{H.c.} \right), \quad (1)$$

where the EBHM Hamiltonian is given by

$$\begin{aligned} \hat{H}_{\text{EBHM}} = & -t \sum_j \left( \hat{b}_{j+1}^\dagger \hat{b}_j + \text{H.c.} \right) + U \sum_j \hat{n}_j (\hat{n}_j - 1) / 2 \\ & + V \sum_j \hat{n}_j \hat{n}_{j+1}. \end{aligned} \quad (2)$$

Here,  $\hat{b}_j^\dagger$  ( $\hat{b}_j$ ) creates (annihilates) a boson at site  $j$  of a one-dimensional lattice, and  $\hat{n}_j = \hat{b}_j^\dagger \hat{b}_j$  is the corresponding particle number operator. The transfer amplitude  $t$  enables the bosons to hop between neighboring lattice sites, whereas the on-site (nearest-neighbor) Coulomb repulsion  $U$  ( $V$ ) tends to localize the particles by establishing an MI (a DW) ground state, at least when the number of bosons  $N$  equals the number of lattice sites  $L$ , i.e.,  $\rho = N/L = 1$ . In this case, a finite dimerization should also promote an insulating state but now with alternating strong and weak bonds.

The ground-state phase diagram of the pure BHM, where  $V = 0$  and  $\delta = 0$ , has only two phases, an SF and an MI [17], which are separated by a Kosterlitz-Thouless phase transition at  $t/U \simeq 0.305$  for  $\rho = 1$  [18]. Adding now  $V$ , and restricting the maximum number of bosons per site  $n_b$  to be two, the EBHM can be approximately mapped onto the spin-1  $XXZ$  model with

single-ion anisotropy, whereby the bosonic operators  $\hat{b}_j^\dagger$ ,  $\hat{b}_j$ , and  $\hat{n}_j$  will be replaced by the spin-1 operators  $\hat{S}_j^+$ ,  $\hat{S}_j^-$ , and  $\hat{S}_j^z+1$ , respectively [19]. As a result, an SPT Haldane insulator appears between the MI and DW phases for intermediate couplings [11, 20], which resembles the gapped Haldane phase of the quantum spin-1 Heisenberg chain [8]. We note that the HI phase continues to exist if one includes higher boson numbers  $n_b > 2$  [21, 22]. In the DMRG calculations, a finite maximum number of bosons per site  $n_b$  must be used. All results for  $\rho = 1$  in the main text are obtained with  $n_b = 4$ .

To explore the effects of the dimerization in the full model (1), we employ the matrix-product-state-based infinite DMRG (iDMRG) technique [23]. The iDMRG provides us with unbiased numerical data directly in the thermodynamic limit. Hence the phase boundaries can be obtained without any finite-size scaling procedure. On the other hand, we determine the critical behavior by tracking the central charge along the quantum phase transition (QPT) lines through the use of the more standard DMRG technique for finite systems with periodic boundary conditions (PBC). The quantum phase transition itself is characterized by various excitation gaps obtained by combining DMRG and infinite matrix-product-state representation at the boundaries of the system [24, 25]

### III. SYSTEM CHARACTERIZATION

Now we present the physical quantities of interest and explain how they can be simulated within the (i)DMRG framework.

#### A. Entanglement spectrum, central charge and correlation length

To determine SPT states in the model (1), we discuss the so-called entanglement spectrum  $\varepsilon_\alpha$  [26], which can be extracted from the Schmidt decomposition. Dividing the system with  $L$  sites into two subblocks,  $\mathcal{H} = \mathcal{H}_\ell \otimes \mathcal{H}_{L-\ell}$ , and considering the reduced density matrix  $\rho_\ell = \text{Tr}_{L-\ell}[\rho]$  of a sub-block of (arbitrary) length  $\ell < L$ , the entanglement spectrum is given by the singular values  $\lambda_\alpha$  of  $\rho_\ell$  as  $\varepsilon_\alpha = -2 \ln \lambda_\alpha$ . If we split the system into two semi-infinite pieces during the iDMRG simulations, the entanglement levels  $\varepsilon_\alpha$  show a characteristic degeneracy in the SPT phase, as has been demonstrated for the Haldane phase of the spin-1 chain [10].

The entanglement spectrum also yields valuable information about the criticality of the system. For the von Neumann entanglement entropy,  $S_L(\ell) = -\sum_\alpha \lambda_\alpha^2 \ln \lambda_\alpha^2$ , field theory predicts that

$$S_L(\ell) = \frac{c}{3} \ln \left[ \frac{L}{\pi} \sin \left( \frac{\pi \ell}{L} \right) \right] + s_1 \quad (3)$$

in a critical system with PBC [27]. In Eq. (3),  $c$  is the central charge and  $s_1$  is a nonuniversal constant. Employing a doubled unit cell, in view of the explicit dimerization, the central charge can be calculated very efficiently from the relation [28]

$$c^*(L) = \frac{3[S_L(L/2 - 2) - S_L(L/2)]}{\ln\{\cos[\pi/(L/2)]\}}. \quad (4)$$

In addition, within an iDMRG calculation, the correlation length  $\xi_\chi$  can be obtained from the second largest eigenvalue of the transfer matrix for some bond dimension  $\chi$  [16, 23]. While the physical correlation length diverges when the system becomes critical,  $\xi_\chi$  stays finite during the numerical simulations due to the finite bond dimension. Nevertheless,  $\xi_\chi$  can be utilized to determine the phase transition point because it develops a pronounced maximum with increasing  $\chi$  near the critical point. Putting these criteria together, the QPT can be determined with high precision.

#### B. Excitation gaps

To determine the criticality of the QPTs one can simulate various excitation gaps of the model (1), just as for the EBHM [11, 20, 21]. For instance, in the EBHM, the single-particle gap

$$\Delta_{\text{sp}} = E_0(N+1) + E_0(N-1) - 2E_0(N) \quad (5)$$

closes at the MI-HI transition, and the neutral gap

$$\Delta_{\text{n}} = E_1(N) - E_0(N) \quad (6)$$

vanishes at the MI-HI and HI-DW transitions, where  $\Delta_{\text{n}}$  closes linearly in the latter case, indicating a critical exponent  $\nu = 1$  of the Ising universality class. In Eqs. (5) and (6),  $E_0$  ( $E_1$ ) denotes the ground-state energy (energy of the first excited state) of the finite  $L$ -site system with fixed boson number.

#### C. Density-wave order parameter

By analogy with the charge-density-wave order parameter of the fermionic Hubbard-type models [29, 30], a (dimerized) DW state in the model (1) can be characterized by a nonvanishing expectation value of the operator

$$\hat{m}_{\text{DW}} = \frac{1}{L} \sum_j (-1)^j (\hat{n}_j - 1). \quad (7)$$

Most importantly, analyzing  $\langle \hat{m}_{\text{DW}} \rangle$  close to the Ising or the tricritical Ising transition points provides the critical exponent  $\beta$  [30].

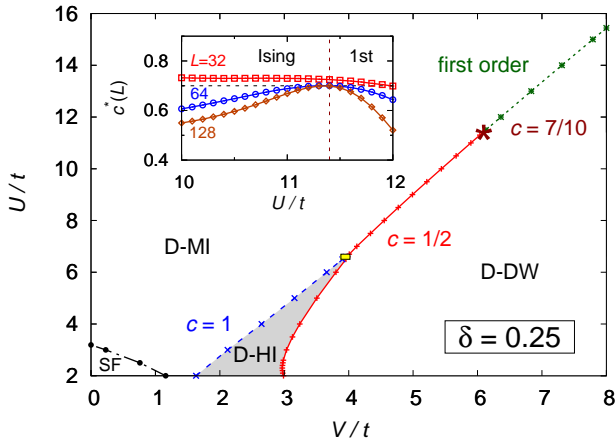


FIG. 1. IDMRG ground-state phase diagram of the dimerized EBHM (1) for  $U/t \geq 2$  with  $\delta = 0.25$  and  $n_b = 4$ . Here the blue dashed line gives the D-MI $\rightleftharpoons$ D-HI phase boundary; the red solid line denotes the continuous Ising phase transition. Both lines merge at the tricritical point located inside the small rectangle which is enlarged in Fig. 4(c) (see also the discussions in the text). The QPT is continuous (first order) below (above) the critical end point  $(V/t, U/t)_{ce}$  marked by the star symbol [there we obtain for the central charge  $c^*(L) \simeq 0.7$  from Eq. (4) as  $L \rightarrow \infty$  on the D-MI $\rightleftharpoons$ D-DW transition line, see inset]. In the weak  $(V, U)$ -coupling regime an SF phase is formed.

#### IV. NUMERICAL RESULTS FOR $\rho = 1$

##### A. Ground-state phase diagram

Figure 1 presents the ground-state phase diagram of the EBHM with an explicit bond dimerization  $\delta = 0.25$  and  $n_b = 4$  obtained by iDMRG. For the considered weak dimerization, we observe, just as for the EBHM ( $\delta = 0$ ), an HI between the MI and DW states, but now these phases exhibit a finite bond dimerization, i.e., actually we have D-HI, D-MI, and D-DW states. For weak onsite and nearest-neighbor repulsions, an SF phase appears. Additionally, there may be a region of phase separation for  $U/t < 2$ , as observed in the model without dimerization [31]. Here, however, we restrict ourselves to the parameter regime  $U/t \geq 2$  in order to concentrate on the study of D-MI, D-HI, and D-DW phases and the transitions between them.

Also the universality classes of the QPT between the D-HI and the D-MI (D-HI and D-DW) phases are the same as for the EBHM, where they are characterized by a central charge  $c = 1$  ( $c = 1/2$ ). The relevant difference is that now the transition between the D-MI and D-DW phases is continuous below a critical end point  $(V/t, U/t)_{ce}$  [which roughly is  $(11.4, 6.08)$  for  $\delta = 0.25$ ]. The continuous transition also belongs to the Ising universality class, except for the critical end point, which belongs to the universality class of the dilute Ising model with  $c = 7/10$ . This will be confirmed numerically below.

##### B. D-HI $\rightleftharpoons$ D-MI and D-HI $\rightleftharpoons$ D-DW quantum phase transitions

We now investigate the nature of the SPT D-HI state and its phase boundaries in more detail. Figure 2(a) displays the behavior of the central charge  $c^*(L)$  as a function of  $V/t$  at fixed  $U/t = 4$ , which is obtained by evaluating Eq. (4) by DMRG for up to  $L = 96$  sites with PBC. Increasing the system size two peaks develop, which indicates the D-MI $\rightleftharpoons$ D-HI and D-HI $\rightleftharpoons$ D-DW transitions. For  $L = 96$ , we find  $c^* \simeq 1.000$  ( $c^* \simeq 0.503$ ) at  $V_{c1}/t \simeq 2.65$  ( $V_{c2}/t \simeq 3.24$ ), which points toward a Gaussian (an Ising) QPT. The corresponding entanglement spectrum  $\varepsilon_\alpha$  [Fig. 2(b)] underlines that a nontrivial topological phase is realized for  $V_{c1} < V < V_{c2}$ , because the entanglement levels show the characteristic degeneracy demonstrated previously for the Haldane phase of the spin-1 chain [10].

Figure 2(c) clearly shows the different behavior of the excitation gaps in the diverse insulator phases, as well as at their phase boundaries: The single-particle gap  $\Delta_{sp}$  is finite throughout the phase diagram, except for the D-HI $\rightleftharpoons$ D-MI QPT, whereas the neutral gap  $\Delta_n$  closes both at the D-MI $\rightleftharpoons$ D-HI and D-HI $\rightleftharpoons$ D-DW QPTs. At the D-HI $\rightleftharpoons$ D-DW transition  $\Delta_n$  closes linearly, which reflects the critical exponent  $\nu = 1$  of the Ising universality class. Nevertheless, the D-HI phase and its phase boundaries display the same behavior as for the nondimerized EBHM. Note that the D-HI phase disappears at the tricritical point  $(V/t, U/t)_{tr}$  [which is located at  $(4.1, 6.9)$  for  $\delta = 0.25$ ], where the central charge becomes 1.

##### C. D-MI $\rightleftharpoons$ D-DW Ising transition

The most significant effect of the dimerization is the direct Ising transition between the D-MI and D-DW phases which could not be observed in the pure EBHM. Figure 3(a) displays the central charge  $c^*(L)$ , obtained from Eq. (4) by DMRG. Obviously, in the vicinity of the D-MI $\rightleftharpoons$ D-DW transition, a peak develops which gets sharper if the system size  $L$  is increased. Fixing  $U/t = 9$ , we find  $c^* \simeq 0.526$  at  $V_c \simeq 4.99$ , indicating that the QPT belongs to the Ising universality class. Since the D-HI phase is absent, the entanglement spectrum  $\varepsilon_\alpha$  is no longer degenerate [in the remaining D-MI and D-DW phases, cf. Fig. 3(b)]. Figure 3(c) gives the excitation gaps for  $U/t = 9$ . Again the single-particle gap  $\Delta_{sp}$  stays finite, and the neutral gap  $\Delta_n$  closes at the D-MI $\rightleftharpoons$ D-DW transition point linearly, i.e.,  $\nu = 1$  (Ising universality class).

As already pointed out, the continuous Ising transition line between D-MI and D-DW phases terminates at the tricritical Ising transition point. The inset of Fig. 1 shows how a pronounced maximum develops in the central charge  $c^*$  on the D-MI $\rightleftharpoons$ D-DW transition line as  $L$  increases. We obtain  $c^* \simeq 0.699$  at the critical end point  $(V/t, U/t)_{ce} \simeq (6.083, 11.4)$ , in agreement with the pre-

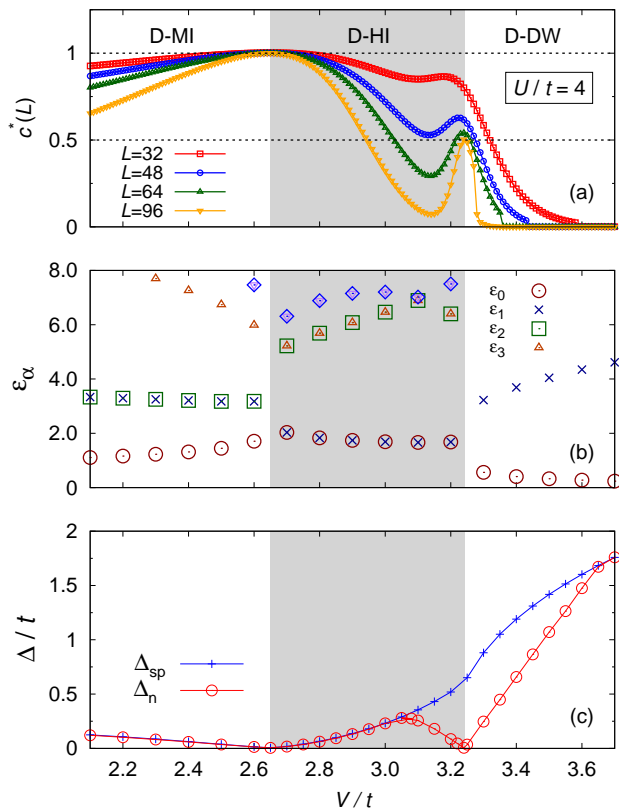


FIG. 2. Central charge (a), entanglement spectrum (b) and excitation gaps (c) of the dimerized EBHM (1) as a function of  $V/t$  at fixed  $U/t = 4$ , where  $\rho = 1$  and  $n_b = 4$ . A central charge  $c = 1$  ( $c = 1/2$ ) indicates the D-HI  $\rightleftharpoons$  D-MI (D-HI  $\rightleftharpoons$  D-DW) transition. The D-HI phase is marked in gray.

diction of field theory for the universality class of the dilute Ising model,  $c = 7/10$ .

#### D. Tricritical regime

To investigate the surroundings of the tricritical point where the D-HI phase vanishes, and determine the value of  $(V/t, U/t)_{tr}$  with maximum precision, we calculated the correlation length  $\xi_\chi$  varying  $V/t$ , at fixed  $U/t$ , above and below the tricritical point. Here a single-peak, respectively, two-peak structure, would be expected. From Fig. 4(a) it seems, however, that in the immediate vicinity of the tricritical point a three-peak structure appears. That is, the DW order parameter  $\langle \hat{m}_{DW} \rangle$  becomes finite not only for  $V > V_{c3}$  but also for  $V_{c1} < V < V_{c2}$  [see Fig. 4(b)], where  $V_{c1} < V_{c2} < V_{c3}$  denote the positions of three peaks. Plotting the position of these peaks when  $U/t$  is changed, we obtain the strongly zoomed-in phase diagram depicted in Fig. 4(c). According to this figure, the D-DW phase penetrates between the D-MI and the D-HI phase near the tricritical point  $(V/t, U/t)_{tr}$ . Since this re-entrance behavior of the D-DW phase is found numerically in a very limited parameter range only,

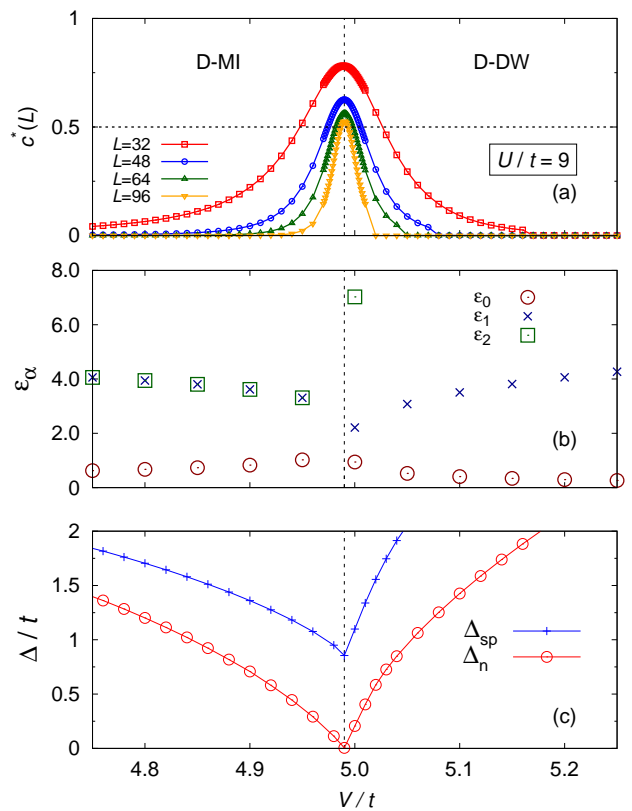


FIG. 3. Central charge (a), entanglement spectrum (b), and excitation gaps (c) of the model (1) as a function of  $V/t$  for fixed  $U/t = 9$  with  $\rho = 1$  and  $n_b = 4$ . The data indicate a D-MI  $\rightleftharpoons$  D-DW transition with  $c = 1/2$ .

and  $V_{c2}$  still shifts in the direction of  $V_{c1}$  as  $\chi$  increases [see Fig. 4(a)], it would be highly desirable to explore this region or behavior more thoroughly, e.g., accompanying our iDMRG calculations by field theory, which is beyond the scope of this work, however.

#### V. SUMMARY AND CONCLUSIONS

In this work we explored the ground-state phase diagram of the extended Bose-Hubbard model with bond dimerization for filling factor  $\rho = 1$  by means of various density-matrix renormalization group techniques. Most notably, we prove the existence of a symmetry-protected-topological (dimerized) HI which separates—at sufficiently weak Coulomb interactions and dimerization—MI and DW states. In addition, we demonstrate a direct Ising transition line between the MI and DW phases for larger Coulomb interactions, which terminates at a tricritical Ising point (end point) with central charge  $c = 7/10$ , where it becomes first order.

The phase diagram of the nondimerized model for  $\rho = 1$  can be understood by analogy to the spin-1  $XXZ$  chain with single-ion anisotropy, with the MI, HI, and DW phases corresponding to the large- $D$ , Haldane, and

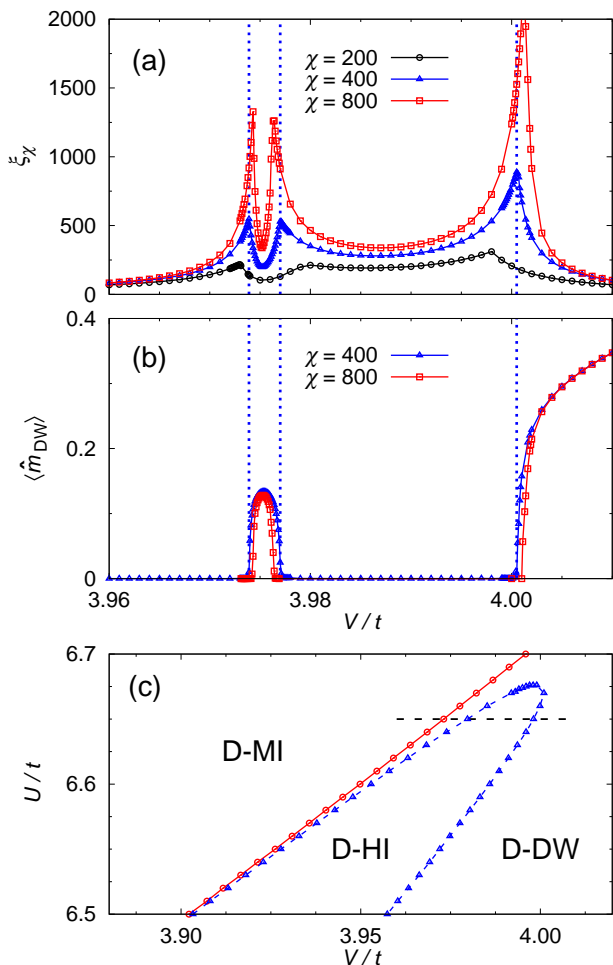


FIG. 4. (a) Three-peak structure of the correlation length  $\xi_\chi$  of the dimerized EBHM with  $\delta = 0.25$  and  $U/t = 6.65$ .  $\chi$  gives the bond dimension used in iDMRG. (b) Corresponding behavior of the DW order parameter  $\langle \hat{m}_{\text{DW}} \rangle$ . Note that  $\langle \hat{m}_{\text{DW}} \rangle$  is finite not only for  $V/t \gtrsim 4.00$  but also for  $3.974 \lesssim V/t \lesssim 3.977$ . The dotted lines denote the QPT points with  $\chi = 400$ . (c) Zoomed-in phase diagram in the immediate vicinity of the tricritical point. The dashed line illustrates the parameter scan performed in panels (a) and (b). Note that the parameter region of panel (c) is equal to the size of the rectangle in Fig. 1.

Néel phases, respectively. In particular, it follows that the HI phase is a symmetry-protected-topological phase, which is protected by a modified bond-centered inversion symmetry [10]. Since this symmetry is respected by the explicit dimerization, the distinction between MI and HI survives in the dimerized model. For weak Coulomb repulsions  $U$  and  $V$ , the system realizes an SF phase, just as for filling factor  $\rho = 1/2$ , where no MI exists at all in the absence of dimerization. If the onsite repulsion  $U$  is sufficiently large in the latter case, adding a small bond dimerization opens an energy gap so that the system passes into a symmetry-protected-topological dimerized MI phase (see Appendix A).

We wish to stress that it is extremely difficult to obtain numerical results with sufficient accuracy in the immediate vicinity of the tricritical point. In consequence, it remains an open question whether the observed intervening dimerized DW will survive the limit of infinite bond dimensions in the infinite density-matrix renormalization group simulation, or the tricritical point will be simply shifted to somewhat greater values of the Coulomb interactions. In order to clarify this issue, an elaborate bosonization-based field theory would be very helpful. Recently, a field theory analysis was carried out in the dimerized spin-1  $XXZ$  chain [32], where the re-entrance behavior of the dimerized Néel phase might also occur.

Equally interesting would be an experimental realization of the dimerized extended Bose-Hubbard model by ultracold atomic gases in optical lattices in order to prove or disprove our theoretical predictions regarding the criticality and nontrivial topological properties.

## ACKNOWLEDGMENTS

We thank T. Yamaguchi for fruitful discussions. K.S. is grateful for the hospitality at the University of Greifswald. F.L. was supported by Deutsche Forschungsgemeinschaft (Germany) through Project No. FE 398/8-1. The iDMRG simulations were performed using the ITensor library [33].

## Appendix A: Case $\rho = 1/2$

At vanishing dimerization and a boson filling factor  $\rho = 1/2$ , a Kosterlitz-Thouless transition occurs between the SF and DW phases, in close analogy to the metal-insulator transition of the fermionic extended Hubbard model at quarter filling [34, 35]. At finite bond dimerization  $\delta$  one expects that the SF phase gives way to an SPT D-MI phase [36]. Then a continuous Ising phase transition might occur between the SPT D-MI and the D-DW (just as in the charge sector of the quarter-filled extended Hubbard model with explicit dimerization [37, 38]). It is well known that the model (1) with  $\rho = 1/2$  can be mapped onto the spin-1/2 dimerized  $XXZ$  model if we take the limit  $U \gg t, V$  and consider only the two lowest Fock states per site  $|0\rangle$  and  $|1\rangle$ . In this case, one may replace  $\hat{b}_j^\dagger, \hat{b}_j$ , and  $\hat{n}_j$  by spin-1/2 operators  $\hat{S}_j^+, \hat{S}_j^-$ , and  $\hat{S}_j^z + 1/2$ , respectively [39], so that the Hamiltonian (1) becomes

$$\hat{H} = -t \sum_j [1 + \delta(-1)^j] (\hat{S}_j^+ \hat{S}_{j+1}^- + \hat{S}_j^- \hat{S}_{j+1}^+) + V \sum_j \hat{S}_j^z \hat{S}_{j+1}^z. \quad (\text{A1})$$

By taking this limit and  $\delta \rightarrow \pm 1$ , the ground state in the D-MI phase can be adiabatically connected to a fully dimerized state with “singlets” at every second bond,

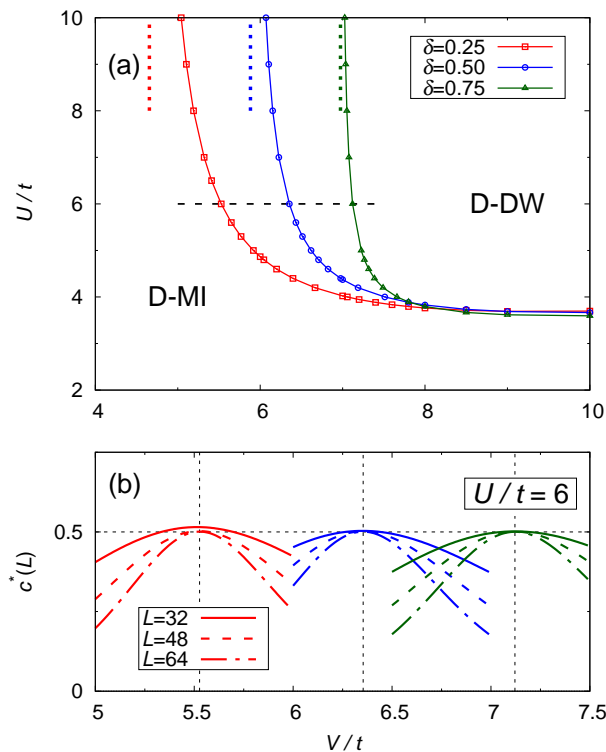


FIG. 5. (a) Ground-state phase diagram of the dimerized EBHM with  $\rho = 1/2$  and  $n_b = 2$ . Data obtained by iDMRG. The dotted lines denote the QPT point with same value of  $\delta$  in the spin-1/2 chain (A1). (b) Central charge  $c^*(L)$  as a function of  $V/t$  at fixed  $U/t = 6$ , calculated [along the dashed line in panel (a)] by finite-system DMRG with PBC.

which implies that the D-MI is an SPT phase protected by inversion symmetry about the strong bonds. This is in contrast to the D-HI for  $\rho = 1$ , which is protected by inversion about both strong and weak bonds, and the D-MI for  $\rho = 1$ , which is a topologically trivial phase.

Figure 5(a) displays the ground-state phase diagram for a maximum number of bosons per site  $n_b = 2$  and different bond dimerizations  $\delta = 0.25, 0.50$ , and  $0.75$ . Only D-MI and D-DW phases appear. The phase boundaries for different  $\delta$  approximately coincide for strong nearest-neighbor interactions  $V/t > 8$ . In the limit  $V \rightarrow \infty$ , the ground state in the D-DW phase becomes a product state with alternating empty and single-occupied sites. The lowest-lying excited state then consists of a single double-occupied site with energy  $U$  and two domain walls with energies  $-2(t + \delta)$  and  $-2(t - \delta)$ . Accordingly, the D-DW state should break down at  $U/t = 4$  for all dimerizations. For smaller  $U/t$ , phase separation should occur

since the D-MI phase is prohibited by the strong nearest-neighbor repulsion. The critical value  $U/t = 4$  roughly agrees with our numerical results for  $V/t \lesssim 10$ . However, in the parameter region studied, the D-DW borders only on the D-MI and no phase separation is observed.

The universality class of the QPT between the D-MI and the D-DW is deduced from the central charge

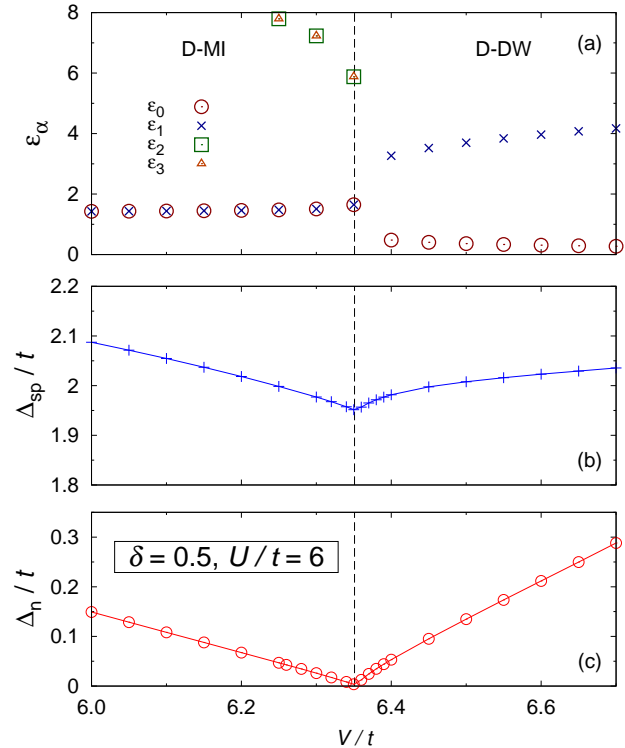


FIG. 6. Entanglement spectrum (a), single-particle gap (b), and neutral gap (c) in the dimerized EBHM with  $\delta = 0.5$  and  $n_b = 2$  at  $U/t = 6$ . The dashed line marks the Ising QPT point at  $V_c/t \simeq 6.351$ .

$c^*(L)$  [Eq. (4)] by DMRG with PBC. The observed value  $c^* \simeq 0.5$  indicates that the transition belongs to the Ising universality class in two dimensions.

Other static properties of the dimerized EBHM are given by Fig. 6 for a bond dimerization  $\delta = 0.5$  and  $U/t = 6$ . Since the D-MI with doubled unit cell is a nontrivial SPT phase, the D-MI entanglement spectrum exhibits the characteristic degeneracy, which is lifted in the D-DW phase. Figure 6(b) gives the single-particle gap for the same parameter set, which has a minimum at the Ising transition point. As in the case of  $\rho = 1$ , the neutral gap  $\Delta_n$  closes linearly at the Ising transition point [see Fig. 6(c)], yielding the critical exponent  $\nu = 1$  of the Ising universality class.

[1] I. Bloch, J. Dalibard, and W. Zwerger, Rev. Mod. Phys. **80**, 885 (2008).

[2] I. Bloch, J. Dalibard, and S. Nascimbène, Nat. Phys. **8**, 267 (2012).

- [3] C. Gross and I. Bloch, *Science* **357**, 995 (2017).
- [4] M. Greiner, O. Mandel, T. Esslinger, T. W. Hänsch, and I. Bloch, *Nature* **415**, 3944 (2002).
- [5] W. Zwerger, ed., *The BCS-BEC Crossover and the Unitary Fermi Gas* (Springer Berlin Heidelberg, 2012).
- [6] S. Baier, M. J. Mark, D. Petter, K. Aikawa, L. Chomaz, Z. Cai, M. Baranov, P. Zoller, and F. Ferlaino, *Science* **352**, 201 (2016).
- [7] R. Landig, L. Hruby, N. Dogra, M. Landini, R. Mottl, T. Donner, and T. Esslinger, *Nature* **532**, 476 (2016).
- [8] F. D. M. Haldane, *Phys. Rev. Lett.* **50**, 1153 (1983).
- [9] Z.-C. Gu and X.-G. Wen, *Phys. Rev. B* **80**, 155131 (2009).
- [10] F. Pollmann, A. M. Turner, E. Berg, and M. Oshikawa, *Phys. Rev. B* **81**, 064439 (2010).
- [11] E. G. Dalla Torre, E. Berg, and E. Altman, *Phys. Rev. Lett.* **97**, 260401 (2006).
- [12] M. Atala, M. Aidelsburger, J. T. Barreiro, D. Abanin, T. Kitagawa, E. Demler, and I. Bloch, *Nat. Phys.* **9**, 795 (2013).
- [13] A. Kitazawa, K. Nomura, and K. Okamoto, *Phys. Rev. Lett.* **76**, 4038 (1996).
- [14] A. Kitazawa and K. Nomura, *J. Phys. Soc. Jpn.* **66**, 3944 (1997).
- [15] S. R. White, *Phys. Rev. Lett.* **69**, 2863 (1992).
- [16] U. Schollwöck, *Ann. Phys.* **326**, 96 (2011).
- [17] T. D. Kühner, S. R. White, and H. Monien, *Phys. Rev. B* **61**, 12474 (2000).
- [18] S. Ejima, H. Fehske, and F. Gebhard, *EPL* **93**, 30002 (2011).
- [19] E. Altman and A. Auerbach, *Phys. Rev. Lett.* **89**, 250404 (2002).
- [20] E. Berg, E. G. Dalla Torre, T. Giamarchi, and E. Altman, *Phys. Rev. B* **77**, 245119 (2008).
- [21] S. Ejima, F. Lange, and H. Fehske, *Phys. Rev. Lett.* **113**, 020401 (2014).
- [22] S. Ejima and H. Fehske, *Phys. Rev. B* **91**, 045121 (2015).
- [23] I. P. McCulloch, arXiv:0804.2509.
- [24] H. N. Phien, G. Vidal, and I. P. McCulloch, *Phys. Rev. B* **86**, 245107 (2012).
- [25] F. Lange, S. Ejima, and H. Fehske, *Phys. Rev. B* **92**, 041120 (2015).
- [26] H. Li and F. D. M. Haldane, *Phys. Rev. Lett.* **101**, 010504 (2008).
- [27] P. Calabrese and J. Cardy, *J. Stat. Mech.* **(2004)**, P06002.
- [28] S. Nishimoto, *Phys. Rev. B* **84**, 195108 (2011).
- [29] S. Ejima, F. H. L. Essler, F. Lange, and H. Fehske, *Phys. Rev. B* **93**, 235118 (2016).
- [30] S. Ejima, F. Lange, F. H. Essler, and H. Fehske, *Physica B: Condensed Matter* **536**, 474 (2018).
- [31] G. G. Batrouni, V. G. Rousseau, R. T. Scalettar, and B. Grémaud, *Phys. Rev. B* **90**, 205123 (2014).
- [32] S. Ejima, T. Yamaguchi, F. H. L. Essler, F. Lange, Y. Ohta, and H. Fehske, *SciPost Phys.* **5**, 59 (2018).
- [33] <http://itensor.org/>.
- [34] F. Mila and X. Zotos, *EPL* **24**, 133 (1993).
- [35] S. Ejima, F. Gebhard, and S. Nishimoto, *EPL* **70**, 492 (2005).
- [36] F. Grusdt, M. Hönig, and M. Fleischhauer, *Phys. Rev. Lett.* **110**, 260405 (2013).
- [37] M. Tsuchiizu and E. Orignac, *J. Phys. Chem. Solids* **63**, 1459 (2002).
- [38] S. Ejima, F. Gebhard, and S. Nishimoto, *Phys. Rev. B* **74**, 245110 (2006).
- [39] E. Altman and A. Auerbach, *Phys. Rev. Lett.* **81**, 4484 (1998).